


## RESEARCH ARTICLE

# Large-eddy simulations of drizzling shallow cumuli using a turbulence-aware autoconversion parametrization

Han-Gyul Jin<sup>1</sup>  | Hyunho Lee<sup>2</sup>  | Jong-Jin Baik<sup>1</sup> <sup>1</sup>School of Earth and Environmental Sciences, Seoul National University, Seoul, South Korea<sup>2</sup>Department of Atmospheric Science, Kongju National University, Gongju, South Korea**Correspondence**Hyunho Lee, Department of Atmospheric Science, Kongju National University, Gongju 32588, South Korea.  
Email: [hyunho.lee@kongju.ac.kr](mailto:hyunho.lee@kongju.ac.kr)**Funding information**

National Research Foundation of Korea, Grant/Award Numbers: 2021R1A2C1007044, 2021R1C1C1012804

**Abstract**

Turbulence in clouds enhances collision between cloud droplets, which is critical to drizzle formation in shallow cumulus clouds. In this study, we develop an autoconversion parametrization that considers the turbulence-induced collision enhancement (TICE) obtained from a particle trajectory model. We implement the developed parametrization to a large-eddy simulation model and simulate the Rain In Cumulus over the Ocean (RICO) case to investigate the effects of TICE on shallow cumulus clouds and their sensitivities to the cloud droplet number concentration and horizontal grid resolution. TICE significantly increases the autoconversion rate, leading to large increases in the accretion rate, rainwater path and surface rain rate. The simulations of shallow cumulus clouds are highly sensitive to the cloud droplet number concentration and horizontal grid resolution, and the inclusion of TICE overall reduces the sensitivities. For example, the large rainwater path and surface rain rate that appear when cloud droplet number concentration is relatively low are reduced by TICE, whereas the very small rainwater path and surface rain rate that appear when cloud droplet number concentration is relatively high are increased by TICE. Comparisons with two other TICE-aware parametrizations based on direct numerical simulation results of droplet collisions in turbulence show that there are substantial differences in TICE effects for different parametrizations, which implies a large uncertainty in simulating turbulent clouds. Among the three parametrizations, the parametrization developed in this study shows intermediate TICE-induced increases in rainwater path and surface rain rate.

**KEYWORDS**

autoconversion parametrization, cloud droplet number concentration, grid resolution, parametrization intercomparison, shallow cumulus cloud, turbulence-induced collision enhancement

## 1 | INTRODUCTION

Turbulence is prevalent in clouds and affects several cloud microphysical processes. Among them, collision and coalescence between cloud droplets is known to be

accelerated by turbulence (e.g. Devenish *et al.*, 2012 and references therein; Grabowski and Wang, 2013 and references therein). Because collision between cloud droplets is critical to raindrop formation, and furthermore, raindrop formation is important to drizzling stratocumuli that

affect radiative forcing as well as to deep convective clouds associated with daily weather prediction and hydrological cycle, the role of turbulence in droplet collisions and raindrop formation should be investigated rigorously.

The enhancement of rate of droplet collisions by turbulence, called hereafter the turbulence-induced collision enhancement (TICE), is thought to result from (1) changes in radial relative velocity between the colliding drops, (2) modification of the flow field around the drops that can increase the collision efficiency and (3) clustering or preferential concentration of drops. Since the pioneering theoretical work by Saffman and Turner (1956), many studies have examined the aforementioned three mechanisms using various methods, such as laboratory experiments (Vohl *et al.*, 1999; Duru *et al.*, 2007; Bordás *et al.*, 2013), direct numerical simulations (DNS) (Franklin *et al.*, 2005; Ayala *et al.*, 2008), theoretical calculations (Ayala *et al.*, 2008) and simulations using a particle trajectory model (Pinsky *et al.*, 2006; 2007). Quantitative discrepancies among the results obtained from different methods are still found, but they are now thought to be moving toward agreement through extensive research for decades.

To investigate how and to what extent TICE affects raindrop formation, surface precipitation and cloud development, numerical models with cloud microphysics schemes that evaluate individual microphysical processes should be employed. Using a two-dimensional (2-D) dynamic model coupled with bin microphysics in which the evolution of hydrometeor size distributions is explicitly evaluated without any predefined shape, Benmoshe *et al.* (2012) performed idealized simulations of deep convective clouds and found that TICE expedites the formation of first raindrops and thus the onset of surface precipitation. Benmoshe and Khain (2014) used the same model and showed that TICE may impact the microphysical structure of clouds more substantially than it does the macrophysical properties such as the accumulated precipitation amount. Lee *et al.* (2014) also conducted idealized simulations of deep mixed-phase convective clouds using the same model as that of Benmoshe and Khain (2014) and showed that the TICE effects are more pronounced when the basic-state wind is vertically uniform than when it is vertically sheared. Through a series of idealized simulations, Lee *et al.* (2015) revealed that the sign of the TICE effects on precipitation from warm-rain cumulus depends on aerosol number concentration. Wyszogrodzki *et al.* (2013) employed a 3-D large-eddy simulation (LES) model coupled with bin microphysics to conduct idealized simulations of drizzling shallow cumuli and showed that TICE leads to earlier raindrop formation and much more production of drizzle. Lee and Baik (2016) conducted a real-case simulation of a heavy precipitation event over the Korean Peninsula using the Weather Research and

Forecasting (WRF) model coupled with bin microphysics and found that surface precipitation is generally increased if TICE is considered. Using the same model as that of Lee and Baik (2016), Lee *et al.* (2018) simulated an idealized shallow cumulus cloud field and showed that changes in complex processes induced by TICE largely offset each other, hence the effects of TICE on cloud radiative properties do not appear prominently.

Although including TICE in bin microphysics models shows promising results toward improving model performance (Lee and Baik, 2016), bin microphysics schemes require huge computational resources, rendering them impractical for use in current operational numerical weather prediction models. As such, including TICE in more computationally efficient bulk microphysics schemes merits a serious investigation. A few studies have attempted to represent TICE in the context of bulk microphysics. Based on Franklin *et al.* (2005), Franklin (2008) proposed a set of warm-rain microphysics parametrizations with explicit dependencies on turbulence-related parameters but without consideration of turbulence effect on collision efficiency. Franklin (2014) updated the autoconversion (AU) parametrization of the developed parametrization set and simulated stratocumulus and shallow cumuli convection fields using an LES model. Seifert *et al.* (2010) improved their former AU parametrization (Seifert and Beheng, 2001, SB01) to be aware of TICE by employing a turbulent collision kernel proposed in Ayala *et al.* (2008), and also simulated a shallow cumuli field. Both studies have shown that the rate of conversion from small cloud droplets to large raindrops, which is evaluated by the AU parametrization in bulk microphysics schemes, is significantly enhanced. However, the two turbulent collision kernels adopted by both studies are based on DNS results in which the Taylor-microscale Reynolds numbers are substantially low. Onishi and Seifert (2016) pointed out that the turbulent collision efficiency in Ayala *et al.* (2008) is likely to be exaggerated due to the extrapolation method applied to the numerical results with low Reynolds numbers.

Recently, Lee and Baik (2017, LB17 hereafter) developed a physically based AU parametrization. They derived the AU rate by analytically evaluating the integrals in the stochastic collection equation in which the collision efficiencies between cloud droplets are obtained using a particle trajectory model (Pinsky *et al.*, 2001). The present study aims to develop an AU parametrization that is based on LB17 and includes TICE obtained using the particle trajectory model in which the drop motion in turbulence is represented as a statistical method (Pinsky *et al.*, 2008). Therefore, it would be beneficial if the elaborate AU parametrization is improved to be TICE-aware, and furthermore, if the TICE-aware AU parametrization

developed using the particle trajectory model, which is free from the low-Reynolds number restriction, is compared with other TICE-aware parametrizations based on DNS results. In this study, a TICE-aware AU parametrization is developed, and large-eddy simulations of shallow cumulus clouds are conducted using the developed AU parametrization. In Section 2, the derivation of the TICE-aware AU parametrization is described. The experimental set-up for the simulations is given in Section 3. The simulation results and the comparison to the simulation without TICE are provided in Section 4. In Section 5, the sensitivities of the simulations to the cloud droplet number concentration and horizontal grid resolution are investigated. In Section 6, the TICE effects obtained using the developed parametrization are compared with those obtained using previous TICE-aware parametrizations. In Section 7, a summary and conclusions are given.

## 2 | DERIVATION

### 2.1 | A summary of LB17

In this subsection, LB17 is summarized to facilitate a description of the derivation of an AU parametrization with TICE. The stochastic growth of drops in clouds is described by the well-known stochastic collection equation (e.g. Pruppacher and Klett, 1997). Lee and Baik (2017) presented the following stochastic collection equation to represent AU:

$$\left. \frac{\partial L_r}{\partial t} \right|_{\text{au}} \approx \frac{4}{3} \pi \rho_w \int_0^\infty \int_0^R (R^3 + r^3) f(r) K(r, R) f(R) dr dR - \alpha \frac{4}{3} \pi \rho_w \int_0^{r^*} \int_0^R (R^3 + r^3) f(r) K(r, R) f(R) dr dR, \quad (1)$$

where  $L_r$  is the rainwater content,  $\rho_w$  is the liquid water density,  $R$  and  $r$  are the radii of cloud droplets,  $r^*$  is the radius that separates cloud droplets from raindrops,  $f(r)dr$  is the number concentration of cloud droplets in the radius interval  $[r, r + dr]$  and  $K$  is the collection kernel. To avoid a slight overestimation of self-collection of cloud droplets, the constant  $\alpha$  is introduced. The value of  $\alpha$  ( $=0.88$ ) is determined from bin microphysics scheme results in the regime where the scheme yields a sufficiently converged solution of the stochastic collection equation (Lee *et al.*, 2019). Equation (1) can be evaluated if  $f(r)$  and  $K(r, R)$  are appropriately given. A gamma-type distribution is usually used to express  $f(r)$  in bulk microphysics schemes:

$$f(r) = N_0 r^\mu \exp(-\lambda r), \quad (2)$$

where  $N_0$  is the intercept parameter,  $\mu$  is the dispersion (or shape) parameter and  $\lambda$  is the slope parameter. In LB17, the dispersion parameter  $\mu$  is not constant but diagnosed following the empirical relation of Thompson *et al.* (2008).

The collection kernel  $K$  is expressed as

$$K(r, R) = \pi(r + R)^2 |v_t(r) - v_t(R)| \eta_g, \quad (3)$$

where  $v_t$  is the terminal velocity of cloud droplets and  $\eta_g$  is the collection efficiency. The collection efficiency is given by the collision efficiency times the coalescence efficiency. The coalescence efficiency is set to be 1; thus, the collection efficiency is equivalent to the collision efficiency. Since only the gravitational effect on collision is taken into account in LB17, the subscript  $g$  is added to  $\eta$ . The terminal velocity of cloud droplets is expressed as  $v_t = v_0 r^2$  following Beard (1976), where  $v_0$  is  $1.0973 \times 10^8$  ( $v_t$  in metres per second and  $r$  in metres). The particle trajectory model of Pinsky *et al.* (2001) is used to calculate the collision efficiency between cloud droplets. The calculated collision efficiency data are used to obtain the following polynomial fitting function:

$$\eta_g(r, R) = k_c \frac{r}{R} \left(1 - \frac{r}{R}\right) \left(\frac{r}{R} + a\right) (R^3 + bR^4), \quad (4)$$

where  $k_c$ ,  $a$  and  $b$  are constant coefficients. The values of  $k_c$ ,  $a$  and  $b$  are  $1.3543 \times 10^{14}$ ,  $2.1421 \times 10^{-1}$  and  $-1.1135 \times 10^4$  ( $r$  and  $R$  in metres), respectively.

Then, for given  $f(r)$  and collection kernel, the integration in Equation (1) can be done analytically to yield the AU rate given by:

$$\left. \frac{\partial L_r}{\partial t} \right|_{\text{au}} = \frac{4}{3} \pi^2 \rho_w N_0^2 v_0 k_c (L_1 - \alpha L_2), \quad (5)$$

where

$$L_1 = \sum_{i=1}^{10} a_i \Gamma_1(\lambda, i) \left[ \Gamma_1(\lambda, 10 - i) - \sum_{j=0}^{\mu+i} \frac{\lambda^j}{j!} \Gamma_1(2\lambda, 10 - i + j) + b \left\{ \Gamma_1(\lambda, 11 - i) - \sum_{j=0}^{\mu+i} \frac{\lambda^j}{j!} \Gamma_1(2\lambda, 11 - i + j) \right\} \right], \quad (6a)$$

$$L_2 = \sum_{i=1}^{10} a_i \Gamma_2(\lambda, i) \left[ \Gamma_2(\lambda, 10 - i) - \sum_{j=0}^{\mu+i} \frac{\lambda^j}{j!} \Gamma_2(2\lambda, 10 - i + j) + b \left\{ \Gamma_2(\lambda, 11 - i) - \sum_{j=0}^{\mu+i} \frac{\lambda^j}{j!} \Gamma_2(2\lambda, 11 - i + j) \right\} \right]. \quad (6b)$$

Here,  $a_i$  ( $i = 1, 2, \dots, 10$ ) is given as  $(a, 1 + a, 1 - 2a, -2 + a, -1 + 2a, 2 - a, -1 - 2a, -2 + a, 1 + a, 1)$ , and  $\Gamma_1(\lambda, n)$  and

$\Gamma_2(\lambda, n)$  are defined as follows:

$$\Gamma_1(\lambda, n) = \frac{(\mu + n)!}{\lambda^{\mu+n+1}}, \quad (7a)$$

$$\Gamma_2(\lambda, n) = \Gamma_1(\lambda, n) \left( 1 - e^{-\lambda r^*} \sum_{k=0}^{\mu+n} \frac{(\lambda r^*)^k}{k!} \right). \quad (7b)$$

From mass conservation, the rate of change of cloud droplet mass content  $\partial L_c / \partial t|_{\text{au}}$  is simply given as  $-\partial L_r / \partial t|_{\text{au}}$ .

The rate of change of cloud droplet number concentration and the rate of change of raindrop number concentration can be derived in a similar way and are given in LB17.

## 2.2 | Inclusion of TICE in LB17

To include TICE in LB17, the improved particle trajectory model developed by Pinsky *et al.* (2007) is used. The model treats the motion of cloud droplets using statistically calculated turbulent shear and Lagrangian acceleration. A detailed description of the model is given in Pinsky *et al.* (2006; 2007). We note that the model usually yields uncorrelated turbulent shear and Lagrangian acceleration and does not treat the fully coupled drop motions and flows, but it can consider relatively high flow Reynolds

number compared to typical DNS models. The model uses the turbulence dissipation rate  $\varepsilon$  and the Taylor microscale Reynolds number  $\text{Re}_\lambda$  as measures of turbulence intensity. A number of experiments with different  $\varepsilon$ – $\text{Re}_\lambda$  pairs using this model show that TICE depends much more strongly on  $\varepsilon$  than on  $\text{Re}_\lambda$  (not shown), which is in agreement with previous studies done using a large-domain DNS model (Onishi and Seifert, 2016). Therefore, for this derivation, we use the results of six experiments with doubling  $\varepsilon$  (50, 100, 200, 400, 800, 1,600  $\text{cm}^2 \cdot \text{s}^{-3}$ ) where  $\text{Re}_\lambda$  is determined according to  $\varepsilon$  following Wyszogrodzki *et al.* (2013), using the relation  $\text{Re}_\lambda = \text{Re}_0(\varepsilon/\varepsilon_0)^{1/6}$  with  $\varepsilon_0 = 100 \text{ cm}^2 \cdot \text{s}^{-3}$  and  $\text{Re}_0 \sim 10,000$ . The enhanced collision efficiency is then calculated using Equation (3) but with  $\eta_g$  being replaced by  $\eta$ . Here,  $\eta$  is the collision efficiency that includes the turbulence effect, and TICE can be represented as  $\eta/\eta_g$ .

The calculated TICE as a function of  $r/R$  and  $R$  for each experiment is shown in Figure 1. As expected, TICE increases with increasing  $\varepsilon$ . Since the particle trajectory model can only be validated with cloud droplets whose radii are within 1–21  $\mu\text{m}$  range (Pinsky *et al.*, 2008), TICE for cloud droplets whose radii are larger than 21  $\mu\text{m}$  are extrapolated with an assumption that TICE is unity for cloud droplets with the 40  $\mu\text{m}$  radius. Note that the TICE value of unity means no turbulent effect and that the turbulent effect is negligible for drops with radii larger than 40  $\mu\text{m}$ . The cloud droplet size at which the TICE value becomes almost unity is uncertain. The two DNS results of

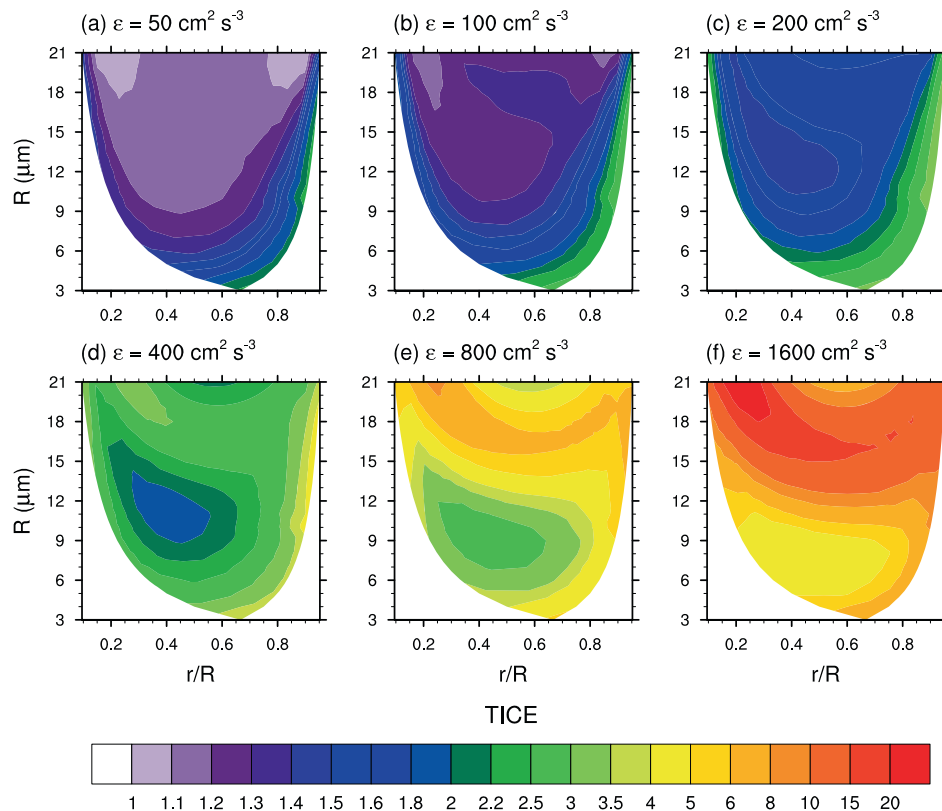


**FIGURE 1**  
Turbulence-induced collision enhancement as a function of  $r/R$  and  $R$  for various turbulent dissipation rates:  $\varepsilon =$  (a) 50, (b) 100, (c) 200, (d) 400, (e) 800 and (f) 1,600  $\text{cm}^2 \cdot \text{s}^{-3}$  [Colour figure can be viewed at [wileyonlinelibrary.com](http://wileyonlinelibrary.com)]



Ayala *et al.* (2008) and Franklin (2008) disagree with each other so that it is  $R \sim 100 \mu\text{m}$  in the Ayala–Wang kernel and  $R \sim 30 \mu\text{m}$  in the Franklin kernel. Because the assumption for the extrapolation may to some extent affect the TICE effects in cloud and precipitation simulations, an update on this assumption may be needed in the future.

The calculated collision efficiency data for each turbulent dissipation rate can be used to obtain the following fitted function which is identical to Equation (4):

$$\eta(r, R; \epsilon) = k_c(\epsilon) \frac{r}{R} \left(1 - \frac{r}{R}\right) \left(\frac{r}{R} + a(\epsilon)\right) (R^3 + b(\epsilon)R^4). \quad (8)$$

Then, using  $k_c$ ,  $a$  and  $b$  data obtained for every  $\epsilon$ , the following fitted functions are obtained:

$$k_c(\epsilon) = \frac{k_0 - k_1}{1 + (\epsilon/k_2)^{k_3}} + k_1, \quad (9)$$

$$a(\epsilon) = a_0 + a_1\epsilon + a_2\epsilon^2 + a_3\epsilon^3, \quad (10)$$

$$b(\epsilon) = (b_0 - b_1) + b_1 \exp\left(-\frac{\epsilon}{b_2}\right), \quad (11)$$

where  $k_i$  and  $a_i$  ( $i = 0, 1, 2$  and  $3$ ) and  $b_i$  ( $i = 0, 1$  and  $2$ ) are constant coefficients, whose values are given in Table 1. The values of  $R^2$  for the fitted functions are 0.9999 for  $k_c$ , 0.9998 for  $a$  and 0.9983 for  $b$ . The AU parametrization that includes TICE has the same form as Equations (5, 6, 7) except that  $k_c$ ,  $a$  and  $b$  are functions of  $\epsilon$ . In the absence of turbulence,  $k_c$ ,  $a$  and  $b$  become identical to those in Equation (4).

### 3 | EXPERIMENTAL SET-UP

The developed parametrization is implemented into the University of California, Los Angeles Large-Eddy Simulation (UCLA-LES) model (Stevens *et al.*, 2005). Using the model, the Rain In Cumulus over the Ocean (RICO) case is simulated to examine how the effects of TICE on shallow cumulus clouds and associated precipitation are described by the developed parametrization. The simulation set-up

mostly follows the experimental protocol of the RICO case given by vanZanten *et al.* (2011). The domain size is  $12.8 \times 12.8 \text{ km}$  in the horizontal with a  $100 \text{ m}$  grid resolution and  $4 \text{ km}$  in the vertical with a  $40 \text{ m}$  grid resolution. Periodic boundary conditions are applied at the lateral boundaries. The surface momentum and thermodynamic fluxes are parametrized using the surface and near-surface values, and the sea-surface temperature is  $299.8 \text{ K}$ . The initial thermodynamic and wind profiles are also taken from vanZanten *et al.* (2011). The model is integrated for  $24 \text{ hr}$ , and the last  $8 \text{ hr}$  data are used for time-average analysis. During the model integration, large-scale forcings such as the large-scale subsidence and net radiative cooling are applied by prescribing time-invariant vertical profiles of subsidence rate, temperature tendency and moisture tendency, as given in vanZanten *et al.* (2011). The cloud microphysical processes are represented by the warm-rain microphysics scheme of Stevens and Seifert (2008), which uses the collection parametrizations of SB01. The cloud water mass, rainwater mass and raindrop number concentration are prognosed, while the cloud droplet number concentration (CDNC) is fixed to  $70 \text{ mg}^{-1}$ . The subgrid-scale turbulence is represented by the Smagorinsky–Lilly model, which gives the turbulent dissipation rate  $\epsilon$  at each grid point and at each time. The developed parametrization uses this  $\epsilon$  to consider TICE.

Two simulations are conducted and compared in Section 4, one employing the developed AU parametrization that considers TICE instead of the model-default SB01 AU parametrization and the other employing the LB17 AU parametrization that does not consider TICE. These simulations are named wTICE and woTICE, respectively. Note that in the simulations in this study, only the direct effect of enhanced collision between droplets are considered. Other mechanisms associated with turbulence such as supersaturation fluctuations and entrainment mixing can broaden the cloud droplet size distribution (Grabowski and Wang, 2013) and eventually affect the collision–coalescence process, but they are not considered in this study.

To investigate the sensitivity of the simulated TICE effects to CDNC, four additional wTICE–woTICE sets of simulations where CDNC is fixed to  $30, 50, 100$  and  $150 \text{ mg}^{-1}$ , respectively, are conducted. These four simulation sets and the control simulation set are named Nc30, Nc50, Nc100, Nc150 and Nc70, respectively. The sensitivity of the simulated TICE effects to the horizontal grid resolution is also examined, by conducting three additional wTICE–woTICE sets of simulations where the horizontal grid spacing is  $25, 50$  and  $200 \text{ m}$ , respectively. These three simulation sets and the control simulation set are named dx25, dx50, dx200 and dx100, respectively.

**TABLE 1** Constant coefficients of the fitted functions in Equations 9, 10 and 11

	$i = 0$	$i = 1$	$i = 2$	$i = 3$
$k_i$	$1.3543 \times 10^{14}$	$3.2798 \times 10^{15}$	$1.9698 \times 10^3$	$1.3848$
$a_i$	$2.1421 \times 10^{-1}$	$-3.3453 \times 10^{-4}$	$6.6145 \times 10^{-7}$	$-1.1269 \times 10^{-10}$
$b_i$	$-1.1135 \times 10^4$	$1.2538 \times 10^4$	$3.0879 \times 10^2$	

Note:  $k_i$  are in per second,  $a_i$  have no units and  $b_i$  are in per metre.

In Section 6, the TICE effects on shallow cumulus clouds simulated using the developed parametrization are compared to those simulated using the parametrization of Seifert and Onishi (2016; SO16 hereafter) and that of Franklin (2014; F14 hereafter). Of the two TICE-aware parametrizations of SO16, the parametrization used in this study is an updated version of the TICE-aware parametrization of Seifert *et al.* (2010), which uses the turbulent collision kernel of Ayala *et al.* (2008) and Wang *et al.* (2008), and it is called the SO16-AW parametrization hereafter. The SO16-AW parametrization is based on the SB01 AU and accretion (AC) parametrizations, using the same formulations but modifying coefficients in the parametrizations to functions of turbulence parameters such as  $\epsilon$  and  $Re_\lambda$ . The comparison of the simulation using the SO16-AW parametrization and the simulation using the SB01 parametrization gives the TICE effects simulated by the SO16-AW parametrization. The F14 parametrization is an updated version of the TICE-aware parametrization of Franklin (2008), which uses the turbulent collision kernel of Franklin *et al.* (2007) obtained from the direct numerical simulations of droplets in turbulent flows. The AU and AC parametrizations have simple power-law equation forms as those of Khairoutdinov and Kogan (2000), but the coefficients are expressed as functions of  $Re_\lambda$ . The simulation using the F14 parametrization is compared with the simulation using the non-turbulent version of the parametrizations given in Franklin (2008). Note that the new parametrization differs only in the AU parametrization with its non-turbulent counterpart, while the SO16-AW and F14 parametrizations differ in both the AU and AC parametrizations with their non-turbulent counterparts.

#### 4 | TICE EFFECTS ON SHALLOW CUMULUS CLOUDS AND ASSOCIATED PRECIPITATION

To investigate the TICE effects on shallow cumulus clouds and associated precipitation simulated by the developed parametrization, the wTICE simulation is compared with the woTICE simulation. Figure 2 shows the time series of domain-averaged liquid water path (LWP), rainwater path (RWP), surface rain rate and cloud cover in the two simulations. After the spin-up, LWP, RWP and surface rain rate gradually increase throughout the simulation period although their fluctuations in a time scale of approximately or less than 1 hr show quite large amplitudes. The cloud cover does not change much throughout the simulation period, with a slightly increasing tendency. The general behaviours of cloud and precipitation properties agree well with the simulations of the RICO case in previous

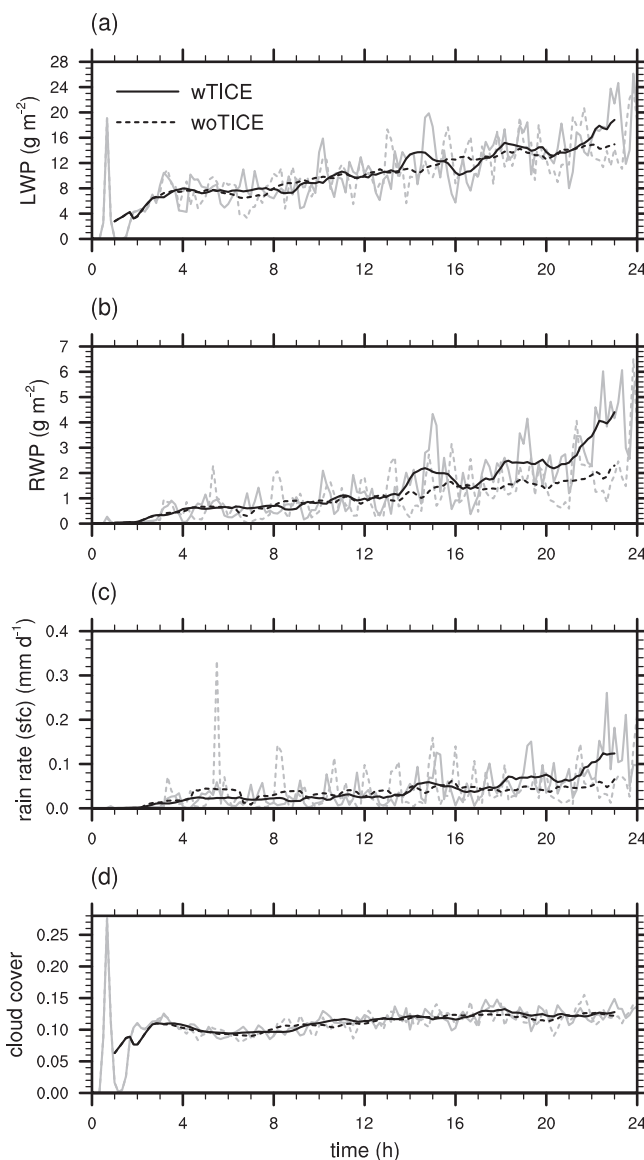


**FIGURE 2** Time series of domain-averaged (a) LWP, (b) RWP, (c) surface rain rate and (d) cloud cover in the wTICE and woTICE simulations. The cloud cover is the fraction of columns that include at least one grid having a cloud water mixing ratio greater than  $0.01 \text{ g kg}^{-1}$ . The black lines indicate the 2 hr moving averages of the time series, and the grey lines indicate the original time series

studies (e.g. vanZanten *et al.*, 2011; F14; SO16). RWP in the wTICE simulation does not deviate much from that in the woTICE simulation until  $t = 13 \text{ hr}$ , but after that, the wTICE simulation shows noticeably larger RWP than the woTICE simulation. This leads to the greater surface rain rate in the wTICE simulation. For the last 8 hr, RWP and surface rain rate in the wTICE simulation are 54% and 44% larger than those in the woTICE simulation, respectively. For the same period, the differences in LWP and cloud cover between the wTICE and woTICE simulations are statistically insignificant at the significance level of 0.05.

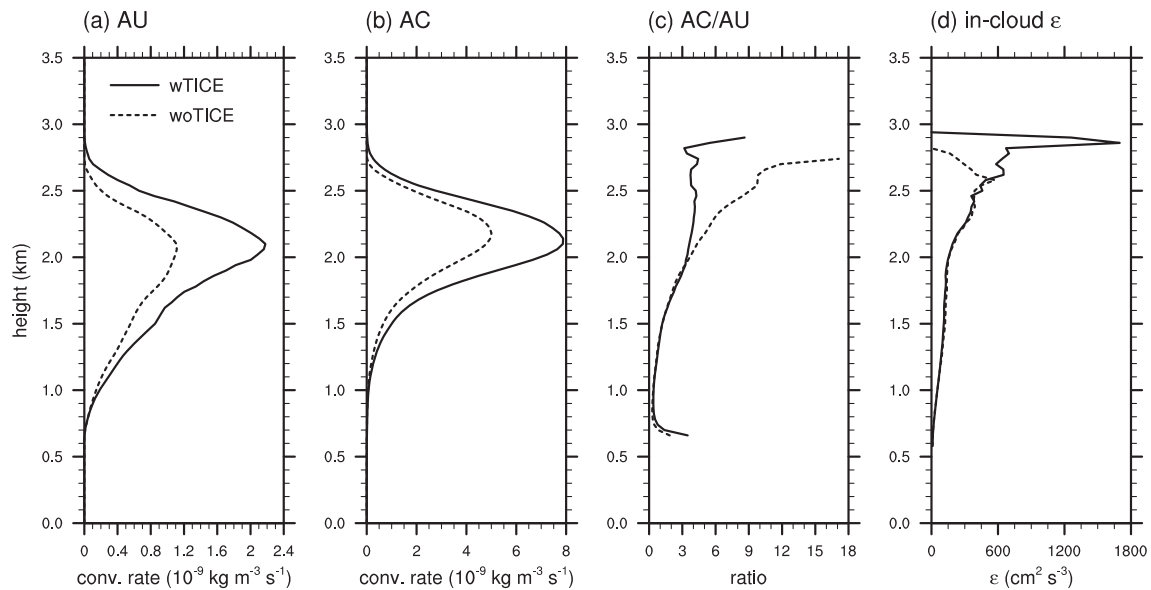


**FIGURE 3** Vertical profiles of (a) AU rate, (b) AC rate, (c) the ratio of AC rate to AU rate (AC/AU) and (d) in-cloud turbulent dissipation rate for the last 8 hr of the wTICE and woTICE simulations. The AU and AC rates are horizontally averaged over the domain and time-averaged. The turbulent dissipation rate is averaged over the grid points where the cloud water mixing ratio is greater than  $0.01 \text{ g} \cdot \text{kg}^{-1}$  and then time-averaged

Obviously, the reason for the larger RWP and surface rain rate in the wTICE simulation is the increase in rain-drop formation due to TICE. Figure 3 shows the vertical profiles of domain-averaged AU rate, AC rate, the ratio of AC rate to AU rate (AC/AU) and in-cloud turbulent dissipation rate. For this case, both the AU and AC play important roles in the rainwater production. These two processes are responsible for 26% and 74% of the total rainwater production, respectively, in the wTICE simulation, and 23% and 77%, respectively, in the woTICE simulation. As a result of the inclusion of TICE in the AU parametrization, the AU rate increases by 81% overall and the increase is maximized at  $z = 2,100 \text{ m}$  (Figure 3a). The region where AU occurs (average AU rate greater than  $10^{-11} \text{ kg} \cdot \text{m}^{-3} \cdot \text{s}^{-1}$ ) is extended 160 m further upward in the wTICE simulation compared to the woTICE simulation. This is associated with the high in-cloud turbulent dissipation rates that appear near the cloud top, which amplifies the TICE effect there (Seifert *et al.*, 2010). The in-cloud turbulent dissipation rate increases with height and is maximized at  $z = 2,880 \text{ m}$  in the wTICE simulation and at  $z = 2,600 \text{ m}$  in the woTICE simulation (Figure 3d). At  $z > 2,600 \text{ m}$ , the in-cloud turbulent dissipation rate in the wTICE simulation is much larger than that in the woTICE simulation.

As the rainwater production via AU increases due to the inclusion of TICE, the AC rate also increases (Figure 3b). In the wTICE simulation, the AC rate is overall greater by 60% and the region where AC occurs is extended further upward compared to the woTICE simulation. However, the increase in the AC rate is not as large as the

increase in the AU rate, which yields a decrease in AC/AU (Figure 3c). In contrast with the woTICE simulation where AC/AU sharply increases with height from  $z \sim 2,000 \text{ m}$ , AC/AU in the wTICE simulation changes only slightly with height above  $z \sim 2,000 \text{ m}$ . This indicates that TICE is the key mechanism that makes AU play an important role in rainwater production near the cloud top. The increase in the AU rate due to TICE leads to a greater production of raindrops that can go through the accretional growth, but at the same time, it also leads to a reduction of cloud droplets to be collected by raindrops. This explains the smaller increase in the AC rate than the increase in the AU rate when TICE is considered. It is noted that SO16 who tested two parametrizations, one based on the Ayala–Wang kernel (Ayala *et al.*, 2008; Wang *et al.*, 2008) and the other based on the Onishi kernel (Onishi *et al.*, 2015), obtained the opposite results, which is an increase in AC/AU, from both parametrizations regardless of CDNC.

Figure 4 shows the vertical profiles of domain-averaged cloud water mixing ratio, rainwater mixing ratio and raindrop number concentration for the last 8 hr of the simulations. The increase in rainwater mixing ratio in the wTICE simulation is maximized at  $z = 2,000 \text{ m}$ , just below the location of maximum increases in the AU rate and AC rate. The relative increase in raindrop number concentration in the wTICE simulation from the woTICE simulation (64%) is greater than that in rainwater mixing ratio (54%) because AU plays a more important role in rainwater production in the wTICE simulation than in the woTICE simulation. This results in a smaller mean size of raindrops

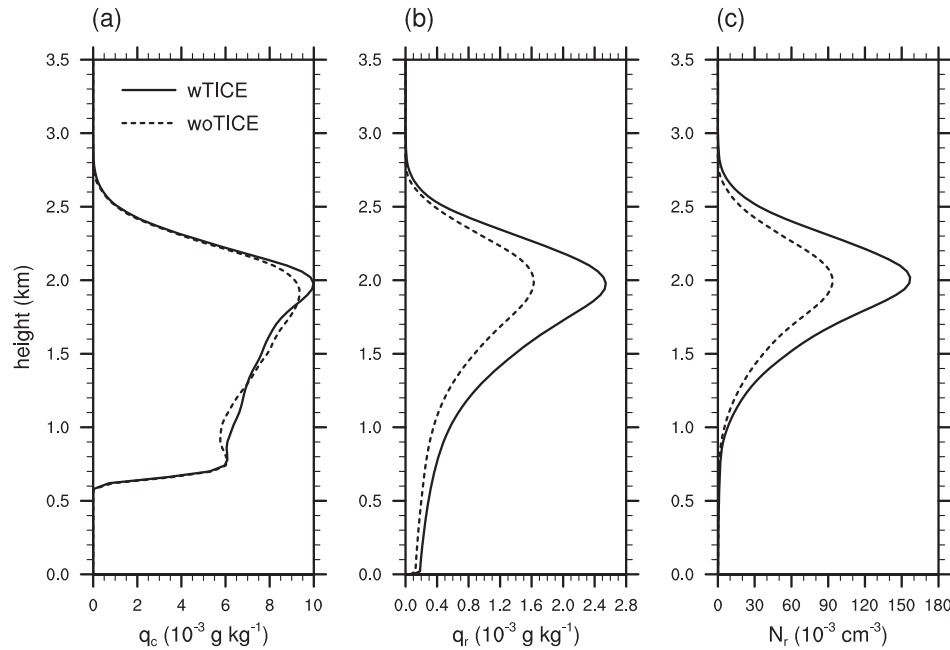


**FIGURE 4** Vertical profiles of horizontally averaged (a) cloud water mixing ratio, (b) rainwater mixing ratio and (c) raindrop number concentration for the last 8 hr of the wTICE and woTICE simulations

in the wTICE simulation. The weaker sedimentation and stronger evaporation of raindrops in the wTICE simulation explain why the increase in surface rain rate (44%) is not as large as the increase in RWP (54%).

Although the conversion to rainwater is much more active in the wTICE simulation, the cloud water mixing ratio in the wTICE and woTICE simulations are almost the same. This indicates that cloud water is more produced in the wTICE simulation possibly because of the “dynamical enhancement” (Wyszogrodzki *et al.*, 2013) that enhances the in-cloud buoyancy. Figure 5 shows the difference vertical profiles of in-cloud liquid water mixing ratio, density potential temperature and vertical velocity between the wTICE and woTICE simulations. The in-cloud liquid water mixing ratio, which is averaged only over the grid points where the liquid water mixing ratio is greater than  $0.01 \text{ g} \cdot \text{kg}^{-1}$ , is reduced at  $z < 2,700 \text{ m}$  in the wTICE simulation because the more active conversion from cloud water to rainwater in the wTICE simulation leads to greater off-loading of condensed water. Note that a substantial increase in the number of in-cloud grid points in the wTICE simulation is the reason for the inconsistency between the decrease in the in-cloud liquid water mixing ratio and the increase in the domain-averaged liquid water mixing ratio. The density potential temperature  $\theta_\rho$ , which includes the condensate loading effects, is calculated following Emanuel (1994) as

$$\theta_\rho = \theta_v \frac{1 + q_v}{1 + q_t}, \quad (12)$$

where  $\theta_v$  is the virtual potential temperature,  $q_t$  is the total water mixing ratio and  $q_v$  is the water vapour mixing

ratio. In the wTICE simulation, the density potential temperature is overall higher at  $z > 1,900 \text{ m}$  where the increase in the AU rate is pronounced. This indicates that the greater off-loading of condensed water increases the in-cloud buoyancy and the buoyancy production of turbulent kinetic energy. The in-cloud vertical velocity overall increases at  $z > 2,100 \text{ m}$  and the increase is prominent at  $z > 2,600 \text{ m}$ . The much greater AU rate at the upper levels in the wTICE simulation may result in prominent dynamical enhancement at those levels, and the enhancement of turbulence can further intensify AU. This could be a positive feedback that leads to a greater vertical development of clouds in the wTICE simulation.

## 5 | SENSITIVITY TESTS

### 5.1 | Sensitivity to cloud droplet number concentration

SO16 have shown that the effects of TICE on cloud and precipitation properties for the RICO case vary with CDNC. However, the developed parametrization may show a different sensitivity to CDNC because of the different turbulent collision kernel used in the parametrization and the different base AU parametrization in which TICE is to be included. In this subsection, we investigate how the developed TICE-aware AU parametrization represents the sensitivity of TICE effects to CDNC.

The cloud and precipitation properties in the wTICE and woTICE simulations with different CDNC are presented in Figure 6. When TICE is not considered, LWP, RWP and surface rain rate largely decrease from Nc30 to



**FIGURE 5** Difference vertical profiles of in-cloud (a) liquid water mixing ratio, (b) density potential temperature and (c) vertical velocity between the wTICE and woTICE simulations (wTICE minus woTICE) for the last 8 hr of the simulations. The density potential temperature and vertical velocity are averaged over the grid points where the cloud water mixing ratio is greater than  $0.01 \text{ g}\cdot\text{kg}^{-1}$  and then time-averaged. The liquid water mixing ratio is averaged over the grid points where the liquid water mixing ratio is greater than  $0.01 \text{ g}\cdot\text{kg}^{-1}$  and then time-averaged

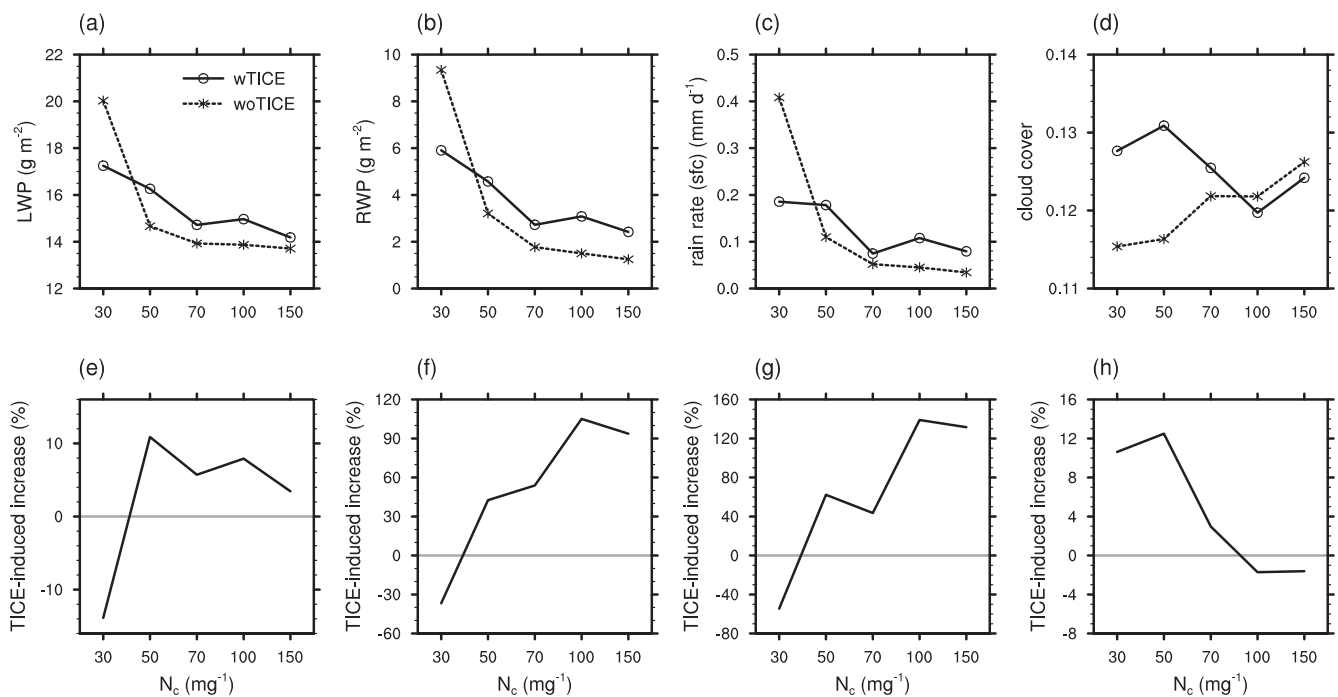
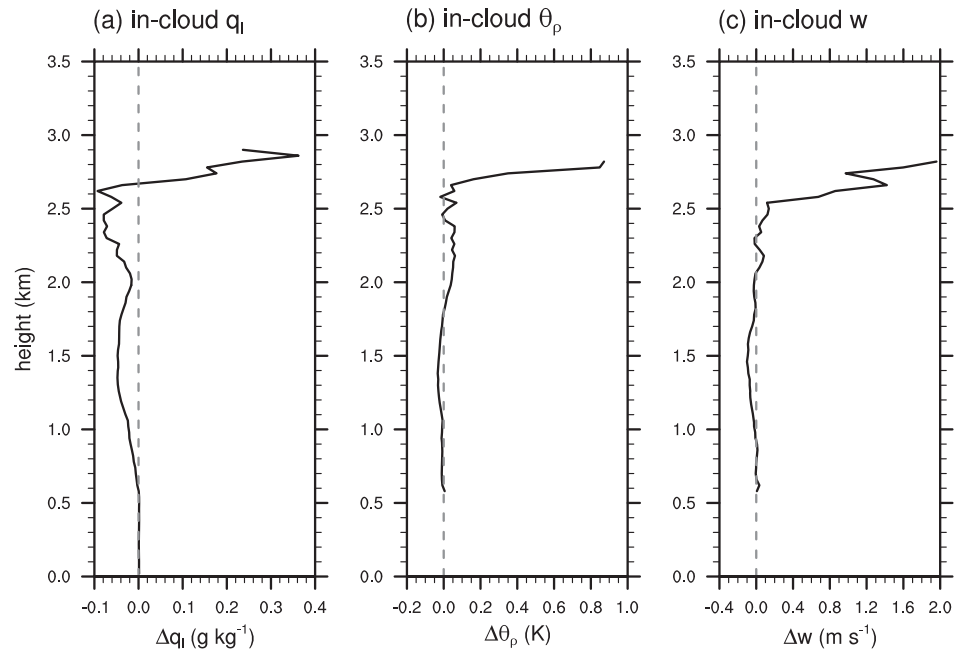


**FIGURE 6** Domain-averaged (a) LWP, (b) RWP, (c) surface rain rate and (d) cloud cover, averaged over the last 8 hr of the simulation period in the wTICE and woTICE simulations with different CDNC. (e–h) The relative differences between the wTICE and woTICE simulations (wTICE minus woTICE)

Nc50 and then gradually decrease with increasing CDNC. When TICE is considered, LWP, RWP and surface rain rate also show a decreasing tendency with increasing CDNC but the decrease from Nc30 to Nc50 is modest. Except for Nc30, the wTICE simulations show greater LWP, RWP and surface rain rate than their counterpart woTICE simulations. Insignificant or negative effects of TICE on RWP and

surface rain rate when CDNC is low were also reported by other modelling studies (e.g. Lee *et al.*, 2015; SO16). The TICE-induced relative change in RWP is very sensitive to CDNC. It is  $-37\%$  for Nc30 and increases with increasing CDNC up to  $105\%$  for Nc100. The TICE-induced change in the surface rain rate shows a similar behaviour to that in RWP. As a result, the sensitivity of RWP and surface

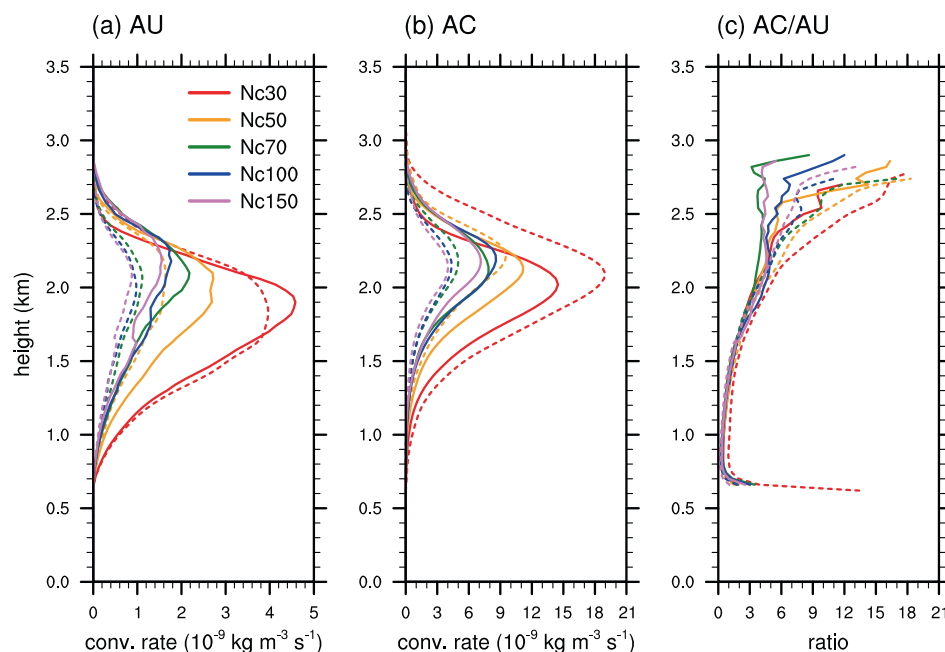


**FIGURE 7** Vertical profiles of (a) AU rate, (b) AC rate and (c) the ratio of AC rate to AU rate (AC/AU) for the last 8 hr of the wTICE (solid lines) and woTICE (dashed lines) simulations with different CDNC. The AU and AC rates are horizontally averaged over the domain and time-averaged [Colour figure can be viewed at [wileyonlinelibrary.com](http://wileyonlinelibrary.com)]

rain rate to CDNC is reduced when TICE is considered; the relative decreases in RWP and surface rain rate from Nc30 to Nc150 in the woTICE simulations are 87% and 92%, respectively, while those in the wTICE simulations are 59% and 57%, respectively. The cloud cover increases due to TICE when CDNC is relatively small (statistically significant increases for Nc30 and Nc50).

Figure 7 shows the vertical profiles of AU rate, AC rate and AC/AU for the last 8 hr of the simulations. As CDNC increases, the AU rate overall decreases and the height of the maximum AU rate rises regardless of the inclusion of TICE. Because the mean size of cloud droplets is larger for lower CDNC, more cloud droplets satisfy the size favourable for AU at relatively low levels, which makes AU occur at relatively low levels and be more active. For high CDNC, cloud droplets are relatively small and they need to reach upper levels to grow large enough to go through AU. The effect of TICE on the AU rate intensifies as CDNC increases. The overall TICE-induced changes in the AU rate for Nc30, Nc50, Nc70, Nc100 and Nc150 are −4%, 51%, 81%, 90% and 92%, respectively. This reflects the weakening of TICE when the mean size of cloud droplets is large. For large droplets with large inertia, gravity dominates their relative motions and their interaction with turbulent airflow is limited. Similar to the AU rate, the AC rate changes due to TICE by −38%, 15%, 60%, 102% and 97% for Nc30, Nc50, Nc70, Nc100 and Nc150, respectively. The sensitivities of AU rate and AC rate to CDNC are responsible for the sensitivity of RWP to CDNC. Except for Nc30, the AU rate and AC rate increase due to TICE, increasing RWP. For Nc30, however, the AC rate decreases significantly due to TICE, which leads to the decreases in RWP and surface

rain rate. For Nc30, the inclusion of TICE increases the AU rate at  $z = 1,680\text{--}2,080\text{ m}$  but decreases the AU rate at upper levels, which is not seen for higher CDNC where the AU rate increases at almost all levels including the upper levels. This indicates that for low CDNC where the mean size of cloud droplets is large and thus AU is very active even without TICE, the additional enhancement of AU due to TICE can act to reduce the raindrop formation at upper levels. The reduction in the raindrop formation at upper levels for low CDNC was also reported by Lee *et al.* (2015). The decrease in the AC rate due to TICE for Nc30 is especially pronounced at the upper levels, which implies that the decrease in the raindrop formation at the upper levels for Nc30 is responsible for it. Regardless of CDNC, AC/AU at upper levels noticeably decrease when TICE is considered.

## 5.2 | Sensitivity to horizontal grid resolution

In this subsection, the sensitivity of the simulated TICE effects to the horizontal grid resolution is examined. The cloud and precipitation properties in the wTICE and woTICE simulations with different horizontal grid resolutions are presented in Figure 8. When TICE is not considered, LWP, RWP and surface rain rate decrease with increasing grid spacing from dx25 to dx100 and increase from dx100 to dx200. The cloud cover decreases with increasing grid spacing from dx25 to dx200. Although these patterns according to the grid resolution do not change despite the inclusion of TICE, the inclusion of

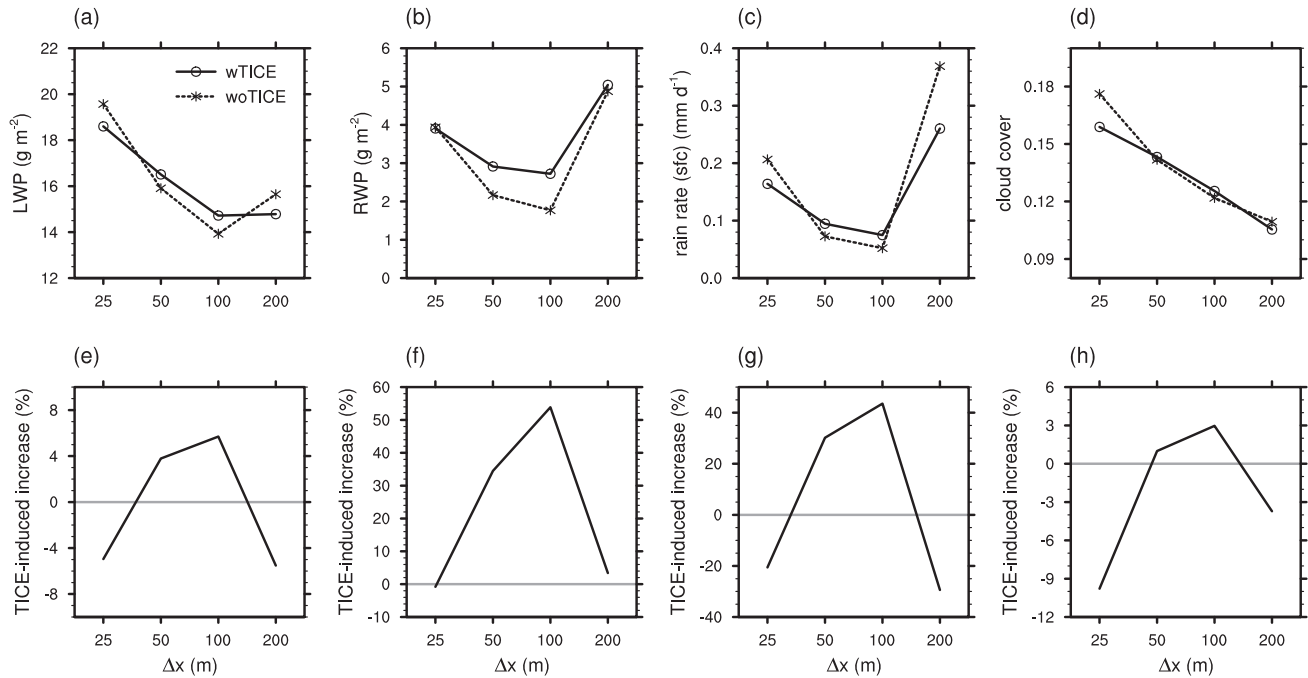


FIGURE 8 As Figure 6 but for different horizontal grid resolutions

TICE weakens the sensitivities of cloud and precipitation properties to the grid resolution. For example, RWP in the wTICE and woTICE simulations are almost the same for dx25, but RWP in the wTICE simulations shows relatively modest decrease from dx25 to dx100 compared to that in the woTICE simulations. The TICE-induced change in RWP (surface rain rate) increases with increasing grid spacing from  $-1\%$  ( $-21\%$ ) for dx25 up to  $54\%$  ( $43\%$ ) for dx100 and decreases to  $3\%$  ( $-29\%$ ) for dx200.

Figure 9 shows the vertical profiles of AU rate, AC rate and AC/AU. Without TICE, the AU rate is relatively large for high-resolution simulations, with dx25 showing the largest AU rate. SO16 attributed this sensitivity of AU rate partly to the high nonlinearity of the AU rate. Because high-resolution simulations better resolve the spatial variability of cloud water mass, the probability distribution of cloud water mixing ratio can be broadened. Given that the AU rate increases dramatically with cloud water mass (e.g. LB17), the broader distribution of cloud water mixing ratio can lead to an increase in the mean AU rate. For dx25, dx50 and dx100, the sensitivity of AC rate in the woTICE simulations is consistent with the sensitivity of AU rate. The AC rate decreases with increasing grid spacing. Also, AC/AU overall decreases with increasing grid spacing for dx25, dx50 and dx100. With TICE, the AU rate in the low-resolution simulations increases substantially.

The overall TICE-induced changes in the AU rate are  $17\%$ ,  $41\%$ ,  $81\%$  and  $74\%$  for dx25, dx50, dx100 and dx200, respectively. The main reason for this sensitivity is the difference in  $\epsilon$ , which the developed AU parametrization

highly depends on. Figure 10a shows the vertical profiles of in-cloud  $\epsilon$ . In-cloud  $\epsilon$  decreases with decreasing grid spacing as more small-scale motions are resolved in grid scale. The overall TICE-induced changes in the AC rate increase with increasing grid spacing for dx25, dx50 and dx100, as those in the AU rate. For dx25, the TICE-induced changes in RWP, surface rain rate, AU rate and AC rate are relatively small, which implies that the importance of the inclusion of TICE in the AU parametrization decreases as the grid refinement becomes high. An interesting point is that dx200 does not follow the trend of TICE-induced changes with grid spacing that is found for dx25, dx50 and dx100. For dx200, the AC rate is largest even when TICE is not considered. This seems to be related to a dynamical effect because dx200 shows much larger in-cloud vertical velocity than the simulations with higher grid resolution, with or without TICE (Figure 10b). The large in-cloud vertical velocity for dx200 keeps aloft some raindrops which would fall out of clouds if the in-cloud vertical velocity were smaller, leading to the large AC rate. Without TICE, AC/AU is largest for dx200, and it decreases substantially when TICE is considered.

## 6 | COMPARISON WITH OTHER TICE PARAMETRIZATIONS

The effects of TICE on shallow cumulus clouds obtained using the developed TICE-aware AU parametrization are compared to those obtained using other TICE-aware

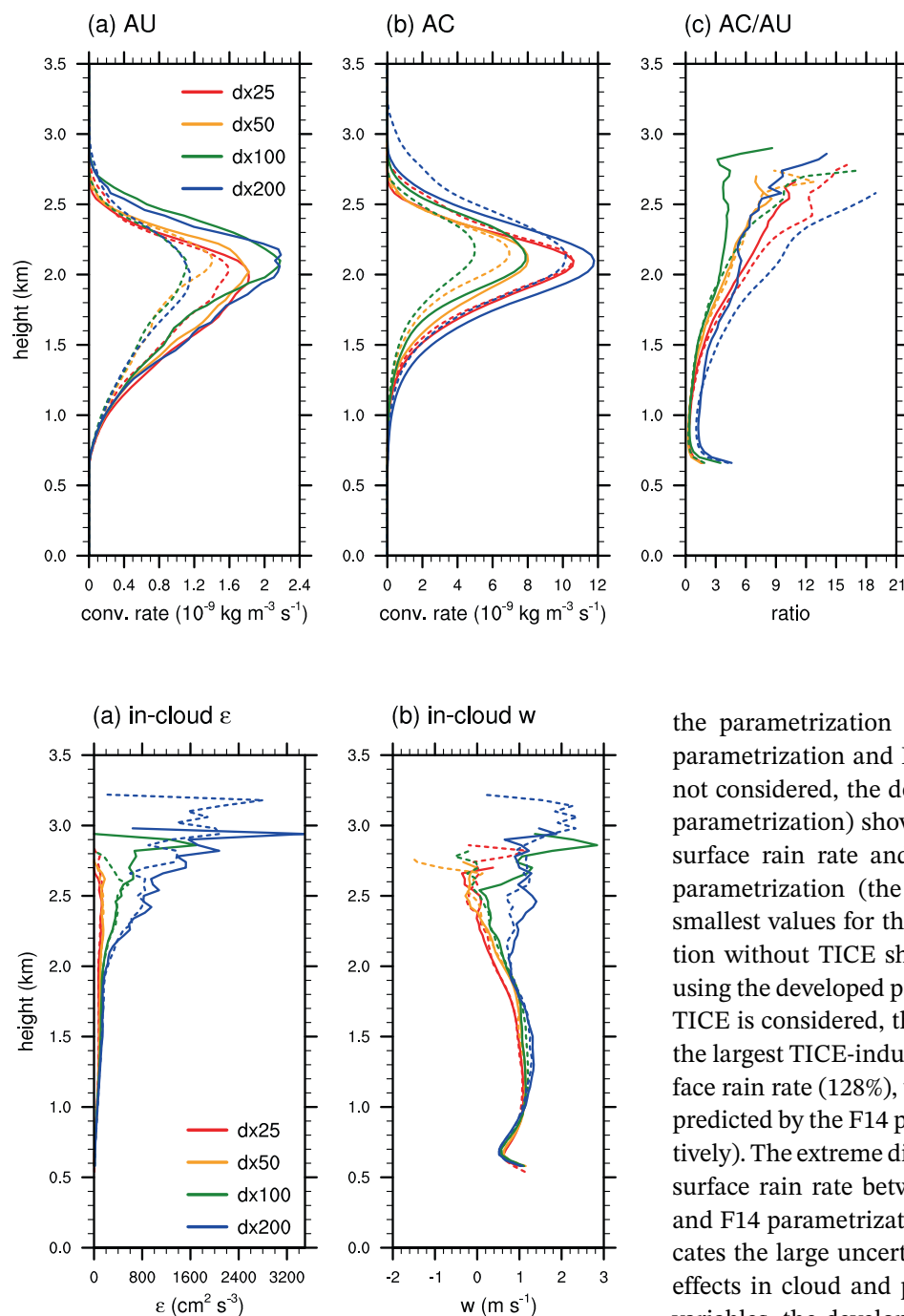


**FIGURE 9** As Figure 7 but for different horizontal grid resolutions [Colour figure can be viewed at [wileyonlinelibrary.com](http://wileyonlinelibrary.com)]

**FIGURE 10** Vertical profiles of (a) in-cloud turbulent dissipation rate and (b) in-cloud vertical velocity for the last 8 hr of the wTICE (solid lines) and woTICE (dashed lines) simulations with different horizontal grid resolutions. The turbulent dissipation rate and vertical velocity are averaged over the grid points where the cloud water mixing ratio is greater than  $0.01 \text{ g kg}^{-1}$  and then time-averaged [Colour figure can be viewed at [wileyonlinelibrary.com](http://wileyonlinelibrary.com)]

parametrizations previously developed based on DNS results. Figure 11 shows the cloud and precipitation properties in the wTICE and woTICE simulations using

the parametrization developed in this study, SO16-AW parametrization and F14 parametrization. When TICE is not considered, the developed parametrization (the LB17 parametrization) shows the largest values for LWP, RWP, surface rain rate and cloud cover, while the SO16-AW parametrization (the SB01 parametrization) shows the smallest values for those variables. The F14 parametrization without TICE shows similar RWP to that predicted using the developed parametrization without TICE. When TICE is considered, the SO16-AW parametrization shows the largest TICE-induced increases in RWP (89%) and surface rain rate (128%), which is in a big contrast with those predicted by the F14 parametrization (22% and 3%, respectively). The extreme difference in TICE effects on RWP and surface rain rate between the SO16-AW parametrization and F14 parametrization both based on DNS results indicates the large uncertainty in the representation of TICE effects in cloud and precipitation simulations. For these variables, the developed parametrization shows intermediate TICE-induced increases (54% and 44%, respectively). For cloud cover, the F14 parametrization shows the largest TICE-induced increase.

The vertical profiles of the cloud microphysical conversion rates are presented in Figure 12. Without TICE, the SO16-AW parametrization shows the smallest AU and AC rates and those predicted by the developed parametrization and F14 parametrization are comparable to each other, which is consistent with the sensitivity of RWP to these parametrizations (Figure 11b). Compared to the F14 parametrization, the developed parametrization shows relatively large AC/AU when TICE is not considered, which explains the larger surface precipitation rate despite



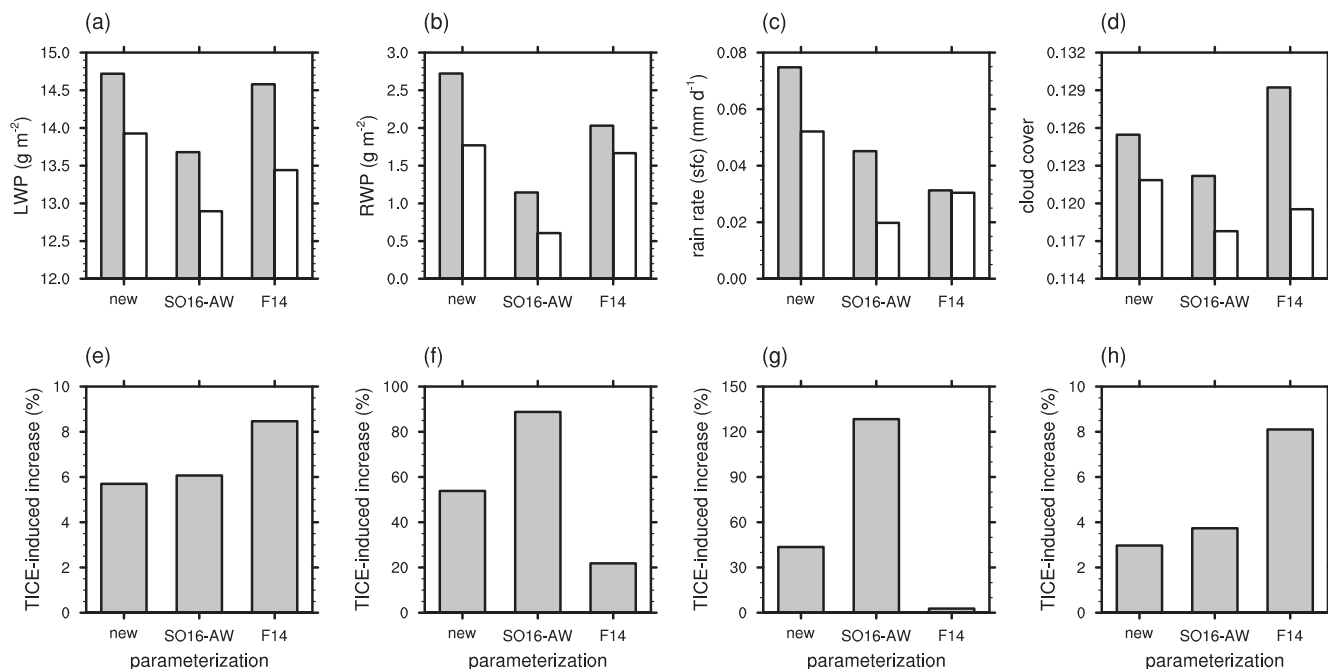
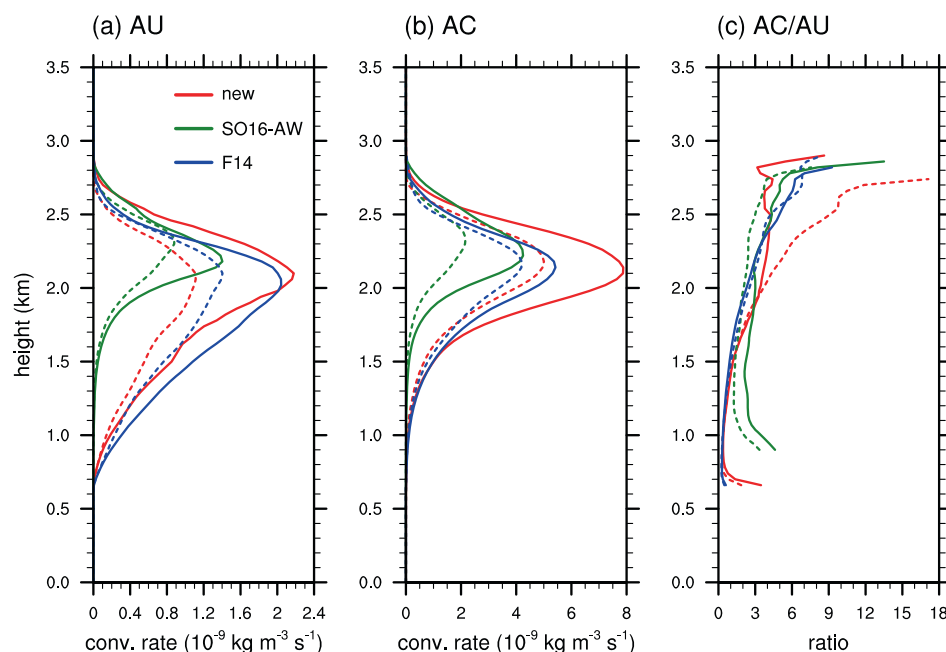


**FIGURE 11** Domain-averaged (a) LWP, (b) RWP, (c) surface rain rate and (d) cloud cover, averaged over the last 8 hr of the simulation period in the wTICE (grey bar) and woTICE (white bar) simulations using different TICE-aware parameterizations. (e–h) The relative differences between the wTICE and woTICE simulations (wTICE minus woTICE)

**FIGURE 12** As Figure 7 but for different TICE-aware parameterizations [Colour figure can be viewed at [wileyonlinelibrary.com](http://wileyonlinelibrary.com)]



similar RWP in the two simulations (Figure 11c). The TICE effect on the AU rate is most prominent for the developed parameterization showing an overall increase by 81%, followed by the SO16-AW parameterization (51%) and F14 parameterization (40%). The overall TICE-induced increase in the AC rate is largest for the SO16-AW parameterization (110%), followed by the developed parameterization (60%) and F14 parameterization (29%). Only the SO16-AW

parameterization shows the increase in the AC rate that is greater than the increase in the AU rate, leading to a substantial increase in AC/AU, which is also shown in SO16. This is responsible for the largest TICE-induced increase in surface rain rate for the SO16-AW parameterization (Figure 11g). In contrast, the F14 parameterization shows a decrease in AC/AU, which is associated with the very small TICE-induced increase in surface rain rate

(Figure 11g) and the largest TICE-induced increase in cloud cover (Figure 11h). The developed parametrization also shows a decrease in AC/AU, which explains the smaller TICE-induced increase in surface rain rate than that in RWP (Figure 11f,g).

## 7 | SUMMARY AND CONCLUSIONS

In this study, we developed a TICE-aware AU parametrization based on the Lee and Baik (2017) AU parametrization, employing TICE obtained using the particle trajectory model of Pinsky *et al.* (2007) that can be applied to relatively high flow Reynolds numbers. Using the developed parametrization, large-eddy simulations of shallow cumulus clouds were conducted. The inclusion of TICE leads to substantial increases in the AU and AC rates and hence large increases in RWP and surface rain rate. The ratio of AC to AU decreases due to TICE, especially at upper levels. The TICE effects are very sensitive to CDNC and horizontal grid resolution. The TICE-induced changes in RWP and surface rain rate are maximum for Nc100 and generally decrease with decreasing CDNC. In terms of the horizontal grid resolution, the TICE-induced changes in RWP and surface rain rate increase with increasing grid spacing until dx100 and then decrease.

Compared to the Seifert and Onishi (2016) parametrization and Franklin (2014) parametrization, which are TICE-aware parametrizations based on DNS results, the simulations using different TICE-aware parametrizations show large differences in the TICE effects on RWP and surface rain rate and the developed parametrization shows intermediate TICE-induced increases in RWP and surface rain rate. The large differences may be attributed to both the differences in turbulent collision kernels obtained from different methods and the differences in base AU parametrization in which TICE is to be included. This indicates that a large uncertainty still exists in simulating turbulent clouds, which should be reduced by further improvement of TICE-aware parametrizations in the future. We note that despite the large difference, all three TICE-aware AU parametrizations as well as the base AU parametrizations compared in this study yield the results within the range proposed in vanZanten *et al.* (2011) owing to the relatively poorly constrained cloud properties. Future research also needs to clarify more proper TICE-aware AU parametrization. The improved understanding and representation of the model uncertainty in the TICE effects on clouds and precipitation brought by the newly suggested parametrization can lead to a careful interpretation of model results and also can enrich prediction through ensemble simulations.

This study exhibits that the sensitivity of simulated cloud and precipitation properties to the horizontal grid resolution decreases when TICE is considered. The sensitivity to the grid resolution partially results from the low-resolution simulation's low capability of representing small-scale phenomena. The decrease in this sensitivity implies that a proper representation of TICE, which reflects the effects of subgrid-scale turbulence on grid-scale cloud properties, may alleviate the uncertainty in numerical simulations of clouds and precipitation.

## AUTHOR CONTRIBUTIONS

**Han-Gyul Jin:** Formal analysis; investigation; validation; visualization; writing – original draft. **Hyunho Lee:** Conceptualization; formal analysis; investigation; methodology; validation; writing – original draft; writing – review and editing. **Jong-Jin Baik:** Conceptualization; formal analysis; supervision; writing – review and editing.

## ACKNOWLEDGEMENTS

We thank two anonymous reviewers for their helpful comments. This work was supported by the National Research Foundation of Korea under grants 2021R1A2C1007044 and 2021R1C1C1012804.

## CONFLICT OF INTEREST

The authors declare no conflict of interest.

## ORCID

Han-Gyul Jin  <https://orcid.org/0000-0001-5618-3529>

Hyunho Lee  <https://orcid.org/0000-0002-7772-5400>

Jong-Jin Baik  <https://orcid.org/0000-0003-3709-0532>

## REFERENCES

- Ayala, O., Rosa, B. and Wang, L.-P. (2008) Effects of turbulence on the geometric collision rate of sedimenting droplets. Part 2. Theory and parameterization. *New Journal of Physics*, 10, 075016.
- Beard, K.V. (1976) Terminal velocity and shape of cloud and precipitation drops aloft. *Journal of the Atmospheric Sciences*, 33, 851–864.
- Benmoshe, N. and Khain, A.P. (2014) The effects of turbulence on the microphysics of mixed-phase deep convective clouds investigated with a 2-D cloud model with spectral bin microphysics. *Journal of Geophysical Research: Atmospheres*, 119, 207–221.
- Benmoshe, N., Pinsky, M., Pokrovsky, A. and Khain, A. (2012) Turbulent effects on the microphysics and initiation of warm rain in deep convective clouds: 2-D simulations by a spectral mixed-phase microphysics cloud model. *Journal of Geophysical Research*, 117, D06220.
- Bordás, R., Roloff, C., Thévenin, D. and Shaw, R.A. (2013) Experimental determination of droplet collision rates in turbulence. *New Journal of Physics*, 15, 045010.

- Devenish, B.J., Bartello, P., Brenguier, J.-L., Collins, L.R., Grabowski, W.W., IJzermans, R.H.A., Malinowski, S.P., Reeks, M.W., Vassilicos, J.C., Wang, L.-P. and Warhaft, Z. (2012) Droplet growth in warm turbulent clouds. *Quarterly Journal of the Royal Meteorological Society*, 138, 1401–1429.
- Duru, P., Koch, D.L. and Cohen, C. (2007) Experimental study of turbulence-induced coalescence in aerosols. *International Journal of Multiphase Flow*, 33, 987–1005.
- Emanuel, K.A. (1994) *Atmospheric Convection*. New York; Oxford: Oxford University Press.
- Franklin, C.N. (2008) A warm rain microphysics parameterization that includes the effect of turbulence. *Journal of the Atmospheric Sciences*, 65, 1795–1816.
- Franklin, C.N. (2014) The effects of turbulent collision-coalescence on precipitation formation and precipitation-dynamical feedbacks in simulations of stratocumulus and shallow cumulus convection. *Atmospheric Chemistry and Physics*, 14, 6557–6570.
- Franklin, C.N., Vaillancourt, P.A. and Yau, M.K. (2007) Statistics and parameterizations of the effect of turbulence on the geometric collision kernel of cloud droplets. *Journal of the Atmospheric Sciences*, 64, 938–954.
- Franklin, C.N., Vaillancourt, P.A., Yau, M.K. and Bartello, P. (2005) Collision rates of cloud droplets in turbulent flow. *Journal of the Atmospheric Sciences*, 62, 2451–2466.
- Grabowski, W.W. and Wang, L.-P. (2013) Growth of cloud droplets in a turbulent environment. *Annual Review of Fluid Mechanics*, 45, 293–324.
- Khairoutdinov, M. and Kogan, Y. (2000) A new cloud physics parameterization in a large-eddy simulation model of marine stratocumulus. *Monthly Weather Review*, 128, 229–243.
- Lee, H. and Baik, J.-J. (2016) Effects of turbulence-induced collision enhancement on heavy precipitation: The 21 September 2010 case over the Korean Peninsula. *Journal of Geophysical Research: Atmospheres*, 121, 319–342.
- Lee, H. and Baik, J.-J. (2017) A physically based autoconversion parametrization. *Journal of the Atmospheric Sciences*, 74, 1599–1616.
- Lee, H., Baik, J.-J. and Han, J.-Y. (2014) Effects of turbulence on mixed-phase deep convective clouds under different basic-state winds and aerosol concentrations. *Journal of Geophysical Research: Atmospheres*, 119, 13506–13525.
- Lee, H., Baik, J.-J. and Han, J.-Y. (2015) Effects of turbulence on warm clouds and precipitation with various aerosol concentrations. *Atmospheric Research*, 153, 19–33.
- Lee, H., Baik, J.-J. and Khain, A.P. (2018) Turbulence effects on precipitation and cloud radiative properties in shallow cumulus: an investigation using the WRF-LES model coupled with bin microphysics. *Asia-Pacific Journal of Atmospheric Sciences*, 54, 457–471.
- Lee, H., Fridlind, A.M. and Ackerman, A.S. (2019) An evaluation of size-resolved cloud microphysics scheme numerics for use with radar observations. Part I: collision-coalescence. *Journal of the Atmospheric Sciences*, 76, 247–263.
- Onishi, R., Matsuda, K. and Takahashi, K. (2015) Lagrangian tracking simulation of droplet growth in turbulence–turbulence enhancement of autoconversion rate. *Journal of the Atmospheric Sciences*, 72, 2591–2607.
- Onishi, R. and Seifert, A. (2016) Reynolds-number dependence of turbulence enhancement on collision growth. *Atmospheric Chemistry and Physics*, 16, 12441–12455.
- Pinsky, M.B., Khain, A.P., Grits, B. and Shapiro, M. (2006) Collisions of small drops in a turbulent flow. Part III: relative droplet fluxes and swept volumes. *Journal of the Atmospheric Sciences*, 63, 2123–2138.
- Pinsky, M.B., Khain, A.P. and Krugliak, H. (2008) Collisions of cloud droplets in a turbulent flow. Part V: application of detailed tables of turbulent collision rate enhancement to simulation of droplet spectra evolution. *Journal of the Atmospheric Sciences*, 65, 357–374.
- Pinsky, M.B., Khain, A.P. and Shapiro, M. (2001) Collision efficiency of drops in a wide range of Reynolds numbers: effects of pressure on spectrum evolution. *Journal of the Atmospheric Sciences*, 58, 742–764.
- Pinsky, M.B., Khain, A.P. and Shapiro, M. (2007) Collisions of cloud droplets in a turbulent flow. Part IV: droplet hydrodynamic interaction. *Journal of the Atmospheric Sciences*, 64, 2462–2482.
- Pruppacher, H.R. and Klett, J.D. (1997) *Microphysics of Clouds and Precipitation*. Dordrecht: Kluwer Academic.
- Saffman, P.G. and Turner, J.S. (1956) On the collision of drops in turbulent clouds. *Journal of Fluid Mechanics*, 1, 16–30.
- Seifert, A. and Beheng, K.D. (2001) A double-moment parameterization for simulating autoconversion, accretion and selfcollection. *Atmospheric Research*, 59–60, 265–281.
- Seifert, A., Nuijens, L. and Stevens, B. (2010) Turbulence effects on warm-rain autoconversion in precipitating shallow convection. *Quarterly Journal of the Royal Meteorological Society*, 136, 1753–1762.
- Seifert, A. and Onishi, R. (2016) Turbulence effects on warm-rain formation in precipitating shallow convection revisited. *Atmospheric Chemistry and Physics*, 16, 12127–12141.
- Stevens, B., Moeng, C.-H., Ackerman, A.S., Bretherton, C.S., Chlond, A., de Roode, S., Edwards, J., Golaz, J.-C., Jiang, H., Khairoutdinov, M., Kirkpatrick, M.P., Lewellen, D.C., Lock, A., Müller, F., Stevens, D.E., Whelan, E. and Zhu, P. (2005) Evaluation of large-eddy simulations via observations of nocturnal marine stratocumulus. *Monthly Weather Review*, 133, 1443–1462.
- Stevens, B. and Seifert, A. (2008) Understanding macrophysical outcomes of microphysical choices in simulations of shallow cumulus convection. *Journal of the Meteorological Society of Japan*, 86A, 143–162.
- Thompson, G., Field, P.R., Rasmussen, R.M. and Hall, W.D. (2008) Explicit forecasts of winter precipitation using an improved bulk microphysics scheme. Part II: implementation of a new snow parameterization. *Monthly Weather Review*, 136, 5095–5115.
- van Zanten, M.C., Stevens, B., Nuijens, L., Siebesma, A.P., Ackerman, A.S., Burnet, F., Cheng, A., Couvreux, F., Jiang, H., Khairoutdinov, M., Kogan, Y., Lewellen, D.C., Mechem, D., Nakamura, K., Noda, A., Shipway, B.J., Slawinska, J., Wang, S. and Wyszogrodzki, A. (2011) Controls on precipitation and cloudiness in simulations of trade-wind cumulus as observed during RICO. *Journal of Advances in Modeling Earth Systems*, 3, M06001.
- Vohl, O., Mitra, S.K., Wurzler, S.C. and Pruppacher, H.R. (1999) A wind tunnel study of the effects of turbulence on the growth of

- cloud drops by collision and coalescence. *Journal of the Atmospheric Sciences*, 56, 4088–4098.
- Wang, L.-P., Ayala, O., Rosa, B. and Grabowski, W.W. (2008) Turbulent collision efficiency of heavy particles relevant to cloud droplets. *New Journal of Physics*, 10, 075013.
- Wyszogrodzki, A.A., Grabowski, W.W., Wang, L.-P. and Ayala, O. (2013) Turbulent collision-coalescence in maritime shallow convection. *Atmospheric Chemistry and Physics*, 13, 8471–8487.

**How to cite this article:** Jin, H.-G., Lee, H. & Baik, J.-J. (2022) Large-eddy simulations of drizzling shallow cumuli using a turbulence-aware autoconversion parametrization. *Quarterly Journal of the Royal Meteorological Society*, 148(749), 3885–3900. Available from: <https://doi.org/10.1002/qj.4395>